9-2006

Data Report: Dissolved sulfide concentration and sulfur isotopic composition of sulfide and sulfate in pore waters, ODP Leg 204, Hydrate Ridge and vicinity, Cascadia margin, offshore Oregon

Walter S. Borowski
Eastern Kentucky University, w.borowski@eku.edu

Tréhu, A.M., Bohrmann, G., Torres, M.E., and Colwell, F.S. (Eds.)
Proceedings of the Ocean Drilling Program, Scientific Results Volume 204

19. Data Report: Dissolved Sulfide Concentration and Sulfur Isotopic Composition of Sulfide and Sulfate in Pore Waters, ODP Leg 204, Hydrate Ridge and Vicinity, Cascadia Margin, offshore Oregon[1]

Walter S. Borowski[2]

ABSTRACT

We report dissolved sulfide sulfur concentrations and the sulfur isotopic composition of dissolved sulfate and sulfide in pore waters from sediments collected during Ocean Drilling Program Leg 204. Porewater sulfate is depleted rapidly as the depth to the sulfate/methane interface (SMI) occurs between 4.5 and 11 meters below seafloor at flank and basin locations. Dissolved sulfide concentration reaches values as high as 11.3 mM in Hole 1251E. Otherwise, peak sulfide concentrations lie between 3.2 and 6.1 mM and occur immediately above the SMI. The sulfur isotopic composition of interstitial sulfate generally becomes enriched in ^{34}S with increasing sediment depth. Peak $\delta^{34}S$-SO_4 values occur just above the SMI and reach up to 53.1‰ Vienna Canyon Diablo Troilite (VCDT) in Hole 1247B. $\delta^{34}S$-ΣHS values generally parallel the trend of $\delta^{34}S$-SO_4 values but are more depleted in ^{34}S relative to sulfate, with values from –12.7‰ to 19.3‰ VCDT. Curvilinear sulfate profiles and carbon isotopic composition of total dissolved carbon dioxide at flank and basin sites strongly suggest that sulfate depletion is controlled by oxidation of sedimentary organic matter, despite the presence of methane gas hydrates in underlying sediments. Preliminary data from

[1]Borowski, W.S., 2006. Data report: Dissolved sulfide concentration and sulfur isotopic composition of sulfide and sulfate in pore waters, ODP Leg 204, Hydrate Ridge and vicinity, Cascadia Margin, offshore Oregon. *In* Tréhu, A.M., Bohrmann, G., Torres, M.E., and Colwell, F.S. (Eds.), *Proc. ODP, Sci. Results,* 204, 1–13 [Online]. Available from World Wide Web: <http://www-odp.tamu.edu/publications/204_SR/VOLUME/CHAPTERS/105.PDF>. [Cited YYYY-MM-DD]
[2]Department of Earth Sciences, Eastern Kentucky University, Richmond KY 40475-3102, USA.
w.borowski@eku.edu

Initial receipt: 10 January 2005
Acceptance: 20 July 2005
Web publication: 28 February 2006
Ms 204SR-105

sulfur species are consistent with this interpretation for Leg 204 sediments at sites not located on or near the crest of Hydrate Ridge.

INTRODUCTION

Sulfur cycling in anoxic marine sediments is complex (e.g., Goldhaber and Kaplan, 1974; Jørgensen, 1983) and is linked to other biogeochemical cycles like that of carbon (Henrichs and Reeburgh, 1987; Valentine and Reeburgh, 2000). Major microbially mediated processes involving sulfur include sulfate reduction (e.g., Berner, 1980; Jørgensen, 1983) and anaerobic methane oxidation (AMO) (Reeburgh, 1983; Valentine and Reeburgh, 2000). Both sulfate reduction and AMO deplete sulfate in pore waters and produce dissolved hydrogen sulfide, ultimately determining the precipitation of sulfide mineral phases, some of which are preserved in the geological record (e.g., Berner, 1980).

Sulfur cycling in sediments overlying significant amounts of gas hydrate may be increasingly influenced by AMO occurring at the base of the sulfate reduction zone or sulfate/methane interface (SMI) (Borowski et al., 2000b; Takacs and Borowski, 2004; Thompson et al., 2004). Ocean Drilling Program Leg 204 sites include those on the flanks of Hydrate Ridge (Sites 1244, 1245, 1246, and 1247), within the sedimentary basin to the east of the feature (Sites 1251 and 1252), and on the crest of the ridge (Sites 1248, 1249, and 1250), where methane is advecting upward at and near the seafloor (Tréhu, Bohrmann, Rack, Torres, et al., 2003; Tréhu et al., 2004). Here we report dissolved sulfide concentration data and sulfur isotopic compositions ($\delta^{34}S$) of dissolved sulfate (SO_4^{2-}) and sulfide (ΣHS) as a first step in assessing the role of AMO in sulfate depletion and investigating other aspects of sulfur cycling in these sediments overlying gas hydrates of the Cascadia margin (Tréhu, Bohrmann, Rack, Torres, et al., 2003; Tréhu et al., 2004).

METHODS

Sediments in the Hydrate Ridge vicinity were collected by coring operations during Leg 204 (Tréhu, Bohrmann, Rack, Torres, et al., 2003). Pore waters were generally extracted and processed using standard methods (Manheim and Sayles, 1974; Tréhu, Bohrmann, Rack, Torres, et al., 2003). At sea, sulfate concentration was determined by ion chromatography, and alkalinity was measured by titration (Gieskes et al., 1991; Tréhu, Bohrmann, Rack, Torres, et al., 2003). The detection limit for both sulfate and alkalinity measurements is <0.1 mM (Gieskes et al., 1991). Other sulfur measurements occurred on shore (see below). A ~3-mL aliquot of pore water was preserved with saturated mercuric chloride (HgCl) solution and flame-sealed within ampoules for carbon isotopic measurements of total dissolved carbon dioxide ($\delta^{34}C$-ΣCO_2) (**Torres and Rugh,** this volume). These $\delta^{34}C$-ΣCO_2 measurements were performed using automated headspace sampling and continuous-flow mass spectroscopy with a precision >0.15‰ (**Torres and Rugh,** this volume).

Dissolved Hydrogen Sulfide

For hydrogen sulfide ($\Sigma HS = H_2S + HS^- + S^{2-}$) concentration measurements, 1 mL of pore water was removed from a secondary syringe

linked to a 50-mL syringe that was directly attached to the squeezing apparatus (D'Hondt, Jørgensen, Miller, et al., 2003) and was injected into a vial containing at least an equal volume of 1.0-M cadmium acetate ($Cd[CH_3CO_2]\cdot 2H_2O$) solution. Assuming a maximum concentration of 30 mM of dissolved sulfide, the trapping solution is concentrated to 33 times in excess for sulfur, assuring the capture of all ΣHS as cadmium sulfide (CdS) precipitate. The precipitate is stable for long periods (T. Lyons, pers. comm., 2003), and ΣHS concentration was measured gravimetrically after the leg. On shore, the preponderance of the trapping solution and pore water sample was decanted. The remaining fluid with its CdS precipitate was progressively diluted and centrifuged to rarefy ions in solution. Then each sample of CdS precipitate was exposed to 10 mL of a composite solution composed of 1-M silver nitrate ($AgNO_3$) and 10% ammonium hydroxide (NH_4OH) (Werne et al., 2003). The CdS precipitate was instantly converted to silver sulfide (Ag_2S) precipitate (Werne et al., 2003), which is very insoluble and resistant to acidification. This Ag_2S precipitate was caught on a 0.1-µm polycarbonate membrane, treated with 5% nitric acid to remove any carbonate solids (pore water samples with sufficient alkalinity are susceptible to forming carbonate precipitate during storage), rinsed repeatedly, dried, and weighed.

Sulfur Isotopic Composition of Dissolved Sulfide

Dissolved sulfide ($\delta^{34}S$-ΣHS) was preserved as CdS within flame-sealed, 7-mL ampoules by placing up to 3 mL of pore water into an approximately equal volume of 1.0-M cadmium acetate solution with a few added drops of saturated HgCl solution. On shore, the pore water and fixative solution was decanted and used for $\delta^{34}S$-SO_4 measurements (see below). The CdS precipitate of each sample was repeatedly rinsed and centrifuged to remove chloride ions (Cl^-) in solution and treated with $AgNO_3$-NH_4OH solution, as described in the section above (Werne et al., 2003). The resultant Ag_2S precipitate was captured on a 0.1-µm polycarbonate filter, stripped of any carbonate precipitate by acidification, and dried. For final preparation for mass spectrometry, Ag_2S precipitate was weighed using a microbalance and placed in tin capsules with vanadium pentoxide (V_2O_5) catalyst. The sulfur isotopic composition of sulfide sulfur was determined after the general method of Holt and Engelkemeir (1970) at Indiana University (USA) using a Finnigan 252 isotope ratio mass spectrometer (Studley et al., 2002). Reproducibility experiments show that the total uncertainty of the extraction process and instrument sensitivity on $\delta^{34}S$-ΣHS measurements is ~0.2‰ Vienna Canyon Diablo Troilite (VCDT).

Sulfur Isotopic Composition of Sulfate

Porewater sulfate ($\delta^{34}S$-SO_4) was obtained by carefully decanting fluid from flame-sealed ampoules prepared as described in the above section. The pore water of each sample was added to 10 mL of a saturated (~1 M), filtered barium chloride ($BaCl_2$) solution. Any dissolved sulfate present was quantitatively precipitated as barium sulfate ($BaSO_4$). The precipitate was filtered on a 0.1-µm polycarbonate filter, repeatedly rinsed with deionized water, and dried. To prepare samples for mass spectrometry, subsamples of the $BaSO_4$ were weighed on a microbalance, added to tin capsules, and combined with V_2O_5. The sulfur isoto-

pic composition of sulfate sulfur was determined using the same procedure as for δ^{34}S-ΣHS (Studley et al., 2002). Reproducibility experiments show that the total uncertainty of the extraction process and instrument sensitivity on δ^{34}S-SO_4 measurements is ~0.1‰ VCDT.

RESULTS

Selected shipboard data and onshore sulfur measurements are tabulated in Table **T1.** Data from sites not located on or near the crest of Hydrate Ridge—the ridge flanks (Sites 1244, 1245, 1246, and 1247) and eastern sedimentary basin (Sites 1251 and 1252)—are graphed in Figure **F1.** Sulfur data from the advective sites of Hydrate Ridge (Sites 1248, 1249, and 1250) are generally sparse and without sufficient resolution to characterize sulfur cycling within these sediments, so these data will not be further addressed in this report.

Pore water concentration and isotopic profiles are generally typical of anoxic marine sediments. Sulfate concentration decreases with increasing sediment depth, exhibiting concave-up profiles. The SMI is defined by low concentrations (<1 mM) of sulfate and rapidly rising methane concentrations (Tréhu, Bohrmann, Rack, Torres, et al., 2003) and occurs between 4.5 (Site 1251) and 11 (Site 1247) meters below seafloor (mbsf). Typically, dissolved sulfide reaches peak concentration at or immediately above the SMI, where it rises as high as 11.3 mM (Hole 1251E), although peak concentrations are generally 3.2–6.1 mM. Alkalinity profiles generally increase with depth until just above or at the SMI, where alkalinity increases with less rapidity. Peak depletion of ^{13}C within total dissolved carbon dioxide (ΣCO_2) also occurs immediately above or at the SMI, with an overall minimum δ^{13}C value of –24.9‰ Vienna Peedee belemnite (VPDB) (Hole 1245B). The sulfur isotopic composition of sulfate generally increases with depth until just above the SMI; the maximum observed value is +53.1‰ VDCT (Hole 1247B), but values usually range between 35.3‰ and 48.0‰. In Holes 1244C and 1245D, δ^{34}S-SO_4 decreases with depth at and below the SMI, showing slight depletions of ^{34}S relative to maximum values. The sulfur isotopic composition of dissolved sulfide also becomes more enriched in ^{34}S with depth and generally parallels the trend of δ^{34}S-SO_4 profiles. The difference in the sulfur isotopic composition of the two species is generally 18.4‰–48.7‰ VCDT, with increasing divergence of δ^{34}S values approaching the SMI. At the SMI and below, δ^{34}S-ΣHS generally reaches stable values of 15.6‰–19.2‰ VCDT.

PRELIMINARY INTERPRETATIONS

Sulfur cycling in marine sediments is complex, although it is essentially controlled by microbially mediated sulfate reduction. Porewater sulfate concentration decreases with sediment depth at all sites because of sulfate reduction. Sulfate containing ^{32}S is preferentially utilized by microbes (e.g., Goldhaber and Kaplan, 1977) so that the sulfur isotopic composition of sulfate becomes more enriched in ^{34}S with depth approaching the SMI. Anomalously, three samples from two holes (1244C and 1245D) show a decrease in δ^{34}S-SO_4 values below maximum values higher in the sulfate reduction zone. This is likely an artifact produced as sulfide is abiotically oxidized to sulfate during handling of samples with very low sulfate concentration. For these samples, dissolved sul-

T1. Dissolved sulfide concentration and sulfur isotopic composition, p. 11.

F1. Concentration and isotopic profiles, p. 9.

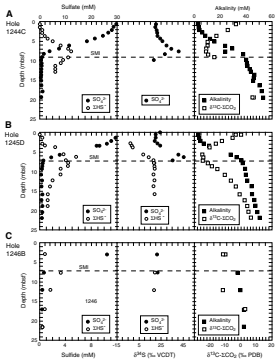

fide is at concentrations several times higher than that of sulfate so that sulfide oxidation is more likely to affect $\delta^{34}S\text{-}SO_4$ values. One sample (9.90 mbsf; Hole 1244C) shows the strongest case for abiotic oxidation, as it has a $\delta^{34}S\text{-}SO_4$ value of 17.9‰—a value less than the accepted sulfur isotopic value of seawater sulfate (21‰) (Rees et al., 1978).

Dissolved sulfide concentrations are controlled by a complex interplay of sulfide production via sulfate reduction and AMO, diffusion of dissolved sulfur species, dissolved sulfide oxidation rates, and iron sulfide mineral precipitation rates, which are in turn governed by availability of dissolved iron (Fe^{2+}) that is determined by iron mineral dissolution (e.g., Werne et al., 2003). Interestingly, peak sulfide concentrations occur immediately above the SMI. Once interstitial sulfate is depleted, sulfate reduction processes and sulfide production cease. Concentration profiles indicate that sulfide produced within the sulfate reduction zone diffuses into the underlying methanogenic zone, presumably because of the lack of dissolved iron needed to form iron sulfide minerals within the sulfate reduction zone. Below the SMI, sulfide is eventually exhausted as it combines with dissolved iron to form iron sulfide minerals. Dissolved iron data (not shown; see Tréhu, Bohrmann, Rack, Torres, et al., 2003) are consistent with this interpretation, generally showing low concentration when dissolved sulfide is present and increases in concentration once sulfide is absent. Microbial transformations of sulfate to sulfide in nature typically exhibit a fractionation factor (α) ranging from 1.029 to 1.059 (e.g., Chambers and Trudinger, 1979). Thus, as expected, the sulfur isotopic composition of dissolved sulfide tracks that of the sulfate pool but is 18.4‰–48.7‰ more depleted in ^{34}S for any particular sample pair. The fractionation involved in forming iron sulfide minerals from dissolved sulfide is only ~1‰ (Price and Shieh, 1979; Wilkin and Barnes, 1996) so that when fractionation caused by sulfate reduction ends, there is little change in $\delta^{34}S\text{-}\Sigma HS$ values below the SMI.

Sulfate depletion in marine sediments is usually controlled by the amount and quality of organic matter deposited within sediments; thus, the oxidation of sedimentary organic matter through sulfate reduction is the prime sulfate-depletion pathway (e.g., Westrich and Berner, 1984; Canfield, 1991; Berner, 1980). A secondary mechanism of sulfate depletion is through AMO, which involves the oxidation of methane and co-consumption of methane and sulfate (Reeburgh, 1983). In some deep-sea sediments associated with methane gas hydrates, AMO is a major sulfate depletion mechanism (see table 4 in Borowski et al., 2000a). For example, AMO is a demonstrably significant process in sediments that overlie gas hydrate deposits of the Blake Ridge region, likely due to low organic matter delivery rates and significant upward flux of methane from underlying gas hydrates (Borowski et al., 1999, 2000a).

Sulfate depletion at the flank and basin sites of Leg 204 seems to be driven by organic matter delivery and oxidation of organic matter through sulfate reduction. A key parameter in assessing the relative significance of sulfate depletion mechanisms in marine sediments is the carbon isotopic composition of ΣCO_2. As most marine sedimentary organic matter has $\delta^{13}C$ more enriched in ^{13}C than –30‰ PDB (Deines, 1980), $\delta^{13}C\text{-}\Sigma CO_2$ values more negative than –30‰ indicate a significant contribution of carbon from methane through AMO (e.g., Reeburgh, 1982; Claypool and Threlkheld, 1983; Borowski et al., 1999). The maximum depletion of ^{13}C in ΣCO_2 in Leg 204 samples collected at

flank and basin locations is –24.9‰ in Hole 1245B (Table T1, Fig. F1) (Torres and Rugh, this volume), strongly suggesting that any contribution of methane carbon via AMO is overwhelmed by carbon donated from sedimentary organic matter through sulfate reduction. Moreover, sulfate profiles are curvilinear (Fig. F1), also suggesting that sulfate depletion is dominated by sulfate reduction rather than AMO in these sediments (Schulz et al., 1994; Borowski et al., 1996).

SUMMARY

1. Dissolved sulfide concentration reaches 11.3 mM (Hole 1251E), but typical maximum values range between 3.2 mM (Hole 1246B) and 6.1 mM (Hole 1247B). Maximum sulfide concentration generally occurs above the SMI.
2. $\delta^{34}S$ values of dissolved sulfate increase with increasing depth into the sulfate reduction zone, reaching maximum values ranging from 35.3‰ (Hole 1252A) to 53.1‰ (Hole 1247B) VCDT.
3. $\delta^{34}S$ values of dissolved sulfide generally mirror the trend of dissolved sulfate but are shifted toward increased ^{34}S depletion by 18.4‰–48.7‰, reaching stable values of 15.6‰ to 19.2 VCDT near the SMI.
4. The carbon isotopic composition of total dissolved carbon dioxide reaches a maximum depletion of –24.9‰ PDBV (Hole 1245B), strongly suggesting that oxidation of sedimentary organic matter is the prime mechanism of interstitial sulfate, rather than anaerobic methane oxidation, despite the presence of gaseous methane and methane gas hydrates in the sediments below. Sulfur concentration and isotopic data are consistent with this interpretation.

ACKNOWLEDGMENTS

This research used samples and/or data provided by the Ocean Drilling Program (ODP). ODP is sponsored by the U.S. National Science Foundation (NSF) and participating countries under management of Joint Oceanographic Institutions (JOI), Inc. Funding for this research was provided by the United States Science Support Program (USSSP). I heartily thank the captain, crew, and technical staff (especially Dennis Graham and Brian Jones) aboard the *JOIDES Resolution* for a most productive leg. Anne Tréhu, Gerhard Bohrmann, Frank Rack, and Marta Torres directed the scientific aspects of Leg 204 with skill and consideration. Tim Lyons provided a wealth of information about preserving dissolved sulfide as CdS and its conversion to Ag_2S. At Indiana University, Lisa Pratt graciously opened her laboratory and Jon Fong provided $\delta^{34}S$ measurements.

REFERENCES

Berner, R.A., 1980. *Early Diagenesis: A Theoretical Approach:* Princeton, NJ (Princeton Univ. Press).

Borowski, W.S., Hoehler, T.M., Alperin, M.J., Rodriguez, N.M., and Paull, C.K., 2000a. Significance of anaerobic methane oxidation in methane-rich sediments overlying the Blake Ridge gas hydrates. *In* Paull, C.K., Matsumoto, R., Wallace, P.J., and Dillon, W.P. (Eds.), *Proc. ODP, Sci. Results,* 164: College Station, TX (Ocean Drilling Program), 87–99.

Borowski, W.S., Paull, C.K., and Ussler, W., III, 1996. Marine pore-water sulfate profiles indicate in situ methane flux from underlying gas hydrate. *Geology,* 24:655–658.

Borowski, W.S., Paull, C.K., and Ussler, W., III, 1999. Global and local variations of interstitial sulfate gradients in deep-water, continental margin sediments: sensitivity to underlying methane and gas hydrates. *Mar. Geol.,* 159:131–154.

Borowski, W.S., Paull, C.K., and Ussler, W., III, 2000b. Geologic implications of sulfide mineralization at the sulfate-methane interface in marine sediments. *Geol. Soc. Am. Bull.,* 32(7):A-256.

Canfield, D.E., 1991. Sulfate reduction in deep-sea sediments. *Am. J. Sci.,* 291:177–188.

Chambers, L.A., and Trudinger, P.A., 1979. Microbiological fractionation of stable sulfur isotopes: a review and critique. *Geomicrobiol. J.,* 1:249–293.

Claypool, G.E., and Threlkeld, C.N., 1983. Anoxic diagenesis and methane generation in sediments of the Blake Outer Ridge, Deep Sea Drilling Project Site 533, Leg 76. *In* Sheridan, R.E., Gradstein, F.M., et al., *Init. Repts. DSDP,* 76: Washington (U.S. Govt. Printing Office), 391–402.

Deines, P., 1980. The isotopic composition of reduced organic carbon. *In* Fritz, P., and Fontes, J.C. (Eds.), *Handbook of Environmental Isotope Geochemistry* (Vol. 1): *The Terrestrial Environment, A:* Amsterdam (Elsevier), 329–406.

D'Hondt, S.L., Jørgensen, B.B., Miller, D.J., et al., 2003. *Proc. ODP, Init. Repts.,* 201 [Online]. Available from World Wide Web: <http://www-odp.tamu.edu/publications/201_IR/201ir.htm>. [Cited 2005-07-08]

Gieskes, J.M., Gamo, T., and Brumsack, H., 1991. Chemical methods for interstitial water analysis aboard *JOIDES Resolution. ODP Tech. Note,* 15 [Online]. Available from World Wide Web: <http://www-odp.tamu.edu/publications/tnotes/tn15/f_chem1.htm>. [Cited 2005-07-08]

Goldhaber, M.B., and Kaplan, I.R., 1974. The sulfur cycle. *In* Goldberg, E.D. (Ed.), *The Sea* (Vol. 5): *Marine Chemistry: The Sedimentary Cycle:* New York (Wiley-Interscience), 569–655.

Henrichs, S.M., and Reeburgh, W.S., 1987. Anaerobic mineralization of marine sediment organic matter: rates and the role of anaerobic processes in the oceanic carbon economy. *J. Geomicrobiol.,* 5:191–237.

Holt, B.D., and Engelkemeir, A.G., 1970. Thermal decomposition of barium sulfate to sulfur dioxide for mass spectrometric analysis. *Anal. Chem.,* 42:1451–1453.

Jørgensen, B.B., 1983. The microbial sulfur cycle. *In* Krumbein, W.E. (Ed.), *Microbial Geochemistry:* St. Louis (Blackwell Scientific Publications), 91–124.

Manheim, F.T., and Sayles, F.L., 1974. Composition and origin of interstitial waters of marine sediments, based on deep sea drill cores. *In* Goldberg, E.D. (Ed.), *The Sea* (Vol. 5): *Marine Chemistry: The Sedimentary Cycle:* New York (Wiley), 527–568.

Price, F.T., and Shieh, Y.N., 1979. Fractionation of sulfur isotopes during laboratory synthesis of pyrite at low temperatures. *Chem. Geol.,* 27:245–253.

Reeburgh, W.S., 1982. A major sink and flux control for methane in marine sediments: anaerobic consumption. *In* Fanning, K.A., and Manheim, F.T. (Eds.), *The Dynamic Environment of the Ocean Floor:* Lexington, MA (D.C. Heath), 203–217.

Reeburgh, W.S., 1983. Rates of biogeochemical processes in anoxic sediments. *Annu. Rev. Earth Planet. Sci.,* 11:269–298.

Rees, C.E., Jenkins, W.J., and Monster, J., 1978. The sulphur isotopic composition of ocean water sulphate. *Geochim. Cosmochim. Acta,* 42:377–381.

Schulz, H.D., Dahmke, A., Schinzel, U., Wallmann, K., and Zabel, M., 1994. Early diagenetic processes, fluxes, and reaction rates in sediments of the South Atlantic. *Geochim. Cosmochim. Acta,* 58:2041–2060.

Studley, S.A., Ripley, E.M., Elswick, E.R., Dorais, M.J., Fong, J., Finkelstein, D., and Pratt, L.M., 2002. Analysis of sulfides in whole rock matrices by elemental analyzer-continuous flow isotope ratio mass spectrometry. *Chem. Geol.,* 192:141–148.

Takacs, K.G., and Borowski, W.S., 2004. Changes in sulfur concentration and sulfur isotopic composition within authigenic sulfide minerals from sediments of Miocene age to the present: ODP Site 995, Blake Ridge, offshore southeastern United States. *Geol. Soc. Am. Bull.,* 36(2):47.

Thompson, M.K., Borowski, W.S., Ussler, W., III, and Paull, C.K., 2004. Sulfide mineralization in deep-water marine sediments related to methane transport, methane consumption, and methane gas hydrates. *Geol. Soc. Am. Bull.,* 36(2):124.

Tréhu, A.M, Bohrmann, G., Rack, F.R., Torres, M.E., et al., 2003. *Proc. ODP, Init. Repts.,* 204 [Online]. Available from World Wide Web: <http://www-odp.tamu.edu/publications/204_IR/204ir.htm>. [Cited 2005-07-08]

Trehu, A.M., Long, P.E., Torres, M.E., Bohrmann, G., Rack, F.R., Collett, T.S., Goldberg, D.S., Milkov, A.V., Riedel, M., Schultheiss, P., Bangs, N.L., Barr, S.R., Borowski, W.S., Claypool, G.E., Delwiche, M.E., Dickens, G.R., Gracia, E., Guerin, G., Holland, M., Johnson, J.E., Lee, Y.-J., Liu, C.-S., Su, X., Teichert, B., Tomaru, H., Vanneste, M., Watanabe, M., and Weinberger, J.L., 2004. Three-dimensional distribution of gas hydrate beneath southern Hydrate Ridge: constraints from ODP Leg 204. *Earth Planet. Sci. Lett.,* 222:845–862.

Valentine, D.L., and Reeburgh, W.S., 2000. New perspectives on anaerobic methane oxidation. *Environ. Microbiol.,* 2:477–484.

Werne, J.P., Lyons, T.W., Hollander, D.J., Formolo, M.J., and Sinninghe Damste, J.S., 2003. Reduced sulfur in euxinic sediments of the Cariaco Basin: sulfur isotope constraints on organic sulfur formation. *Chem. Geol.,* 195:159–179.

Westrich, J.T., and Berner, R.A., 1984. The role of sedimentary organic matter in bacterial sulfate reduction: the G model tested. *Limnol. Oceanogr.,* 29:236–249.

Wilkin, R.T., and Barnes, H.L., 1996. Pyrite formation by reactions of iron monosulfides with dissolved inorganic and organic sulfur species. *Geochim. Cosmochim. Acta,* 60:4167–4179.

Figure F1. Concentration and isotopic profiles of selected porewater species. Holes 1245D, 1246B, and 1244C are part of a west-to-east transect across the northern flank of south Hydrate Ridge; Hole 1247B is located on the northwest flank of south Hydrate Ridge closer to its crest; Holes 1251E and 1252A are in the basin to the east of the feature (Tréhu, Bohrmann, Rack, Torres, et al., 2003). Some profiles are augmented with data from other holes of the same site, and these are noted within the figure panels. Alkalinity, sulfate, and sulfide concentrations are in millimolar units (millimoles per liter); alkalinity and sulfate data are from Tréhu, Bohrmann, Rack, Torres, et al. (2003). Note that graph scales for all sites are identical with the exception of the alkalinity scale for Holes 1251E and 1252A. The sulfate/methane interface (SMI) is shown with dashed lines as determined from sulfate and methane concentrations within pore waters (Tréhu, Bohrmann, Rack, Torres, et al., 2003). Carbon and sulfur isotopic composition is expressed in units of permil. Carbon isotopic composition of total dissolved carbon dioxide ($\delta^{13}C$-ΣCO_2) is relative to Peedee Belemnite, Vienna (VPDB) and the values are from **Torres and Rugh** (this volume); sulfur isotopic composition of dissolved sulfide ($\delta^{34}S$-ΣHS) and sulfate ($\delta^{34}S$-SO_4) are relative to Vienna Canyon Diablo Troilite (VCDT). **A.** Hole 1244C. **B.** Hole 1245D. **C.** Hole 1246B. (Continued on next page.)

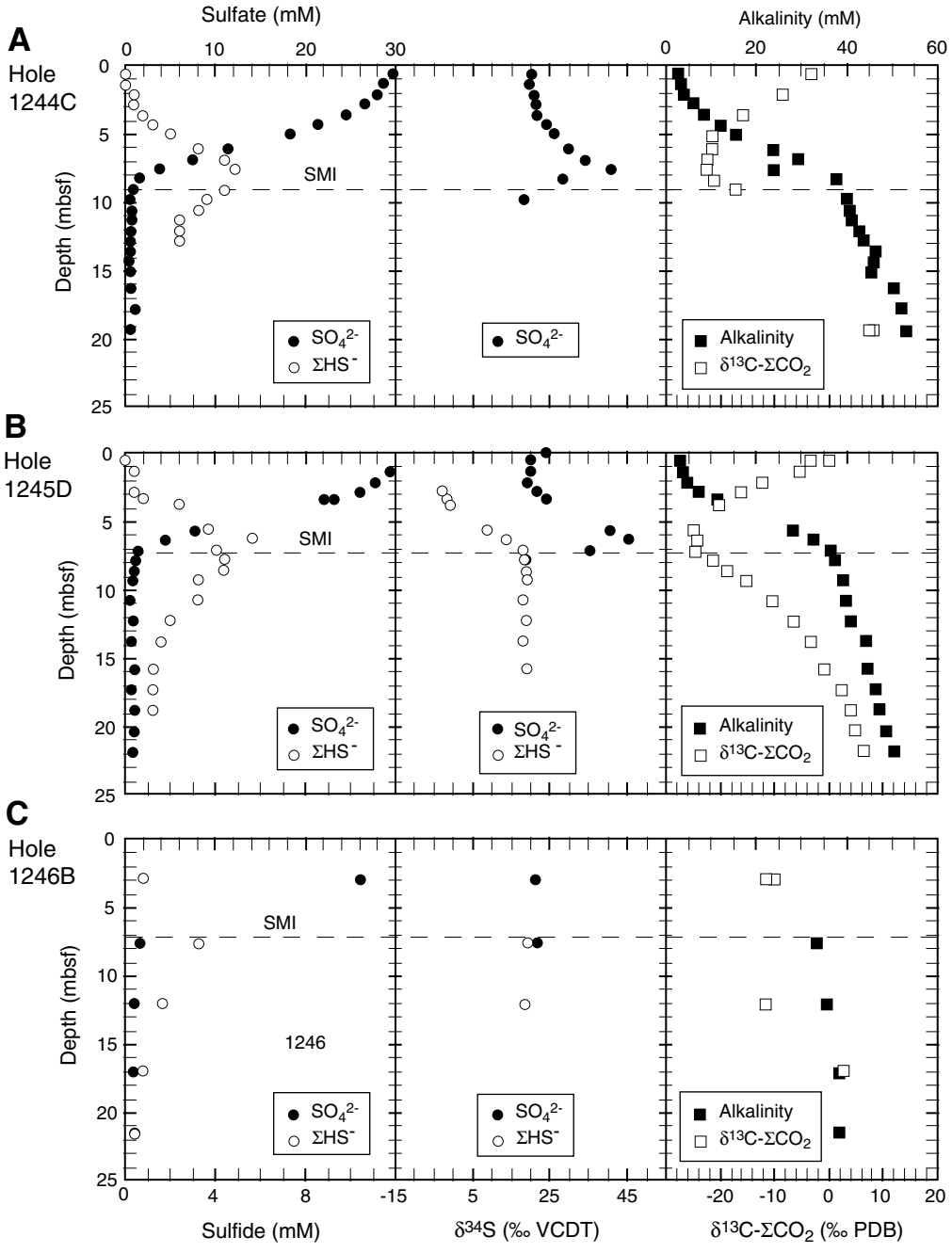

Figure F1 (continued). **D.** Hole 1247B. **E.** Hole 1251E. **F.** Hole 1252A.

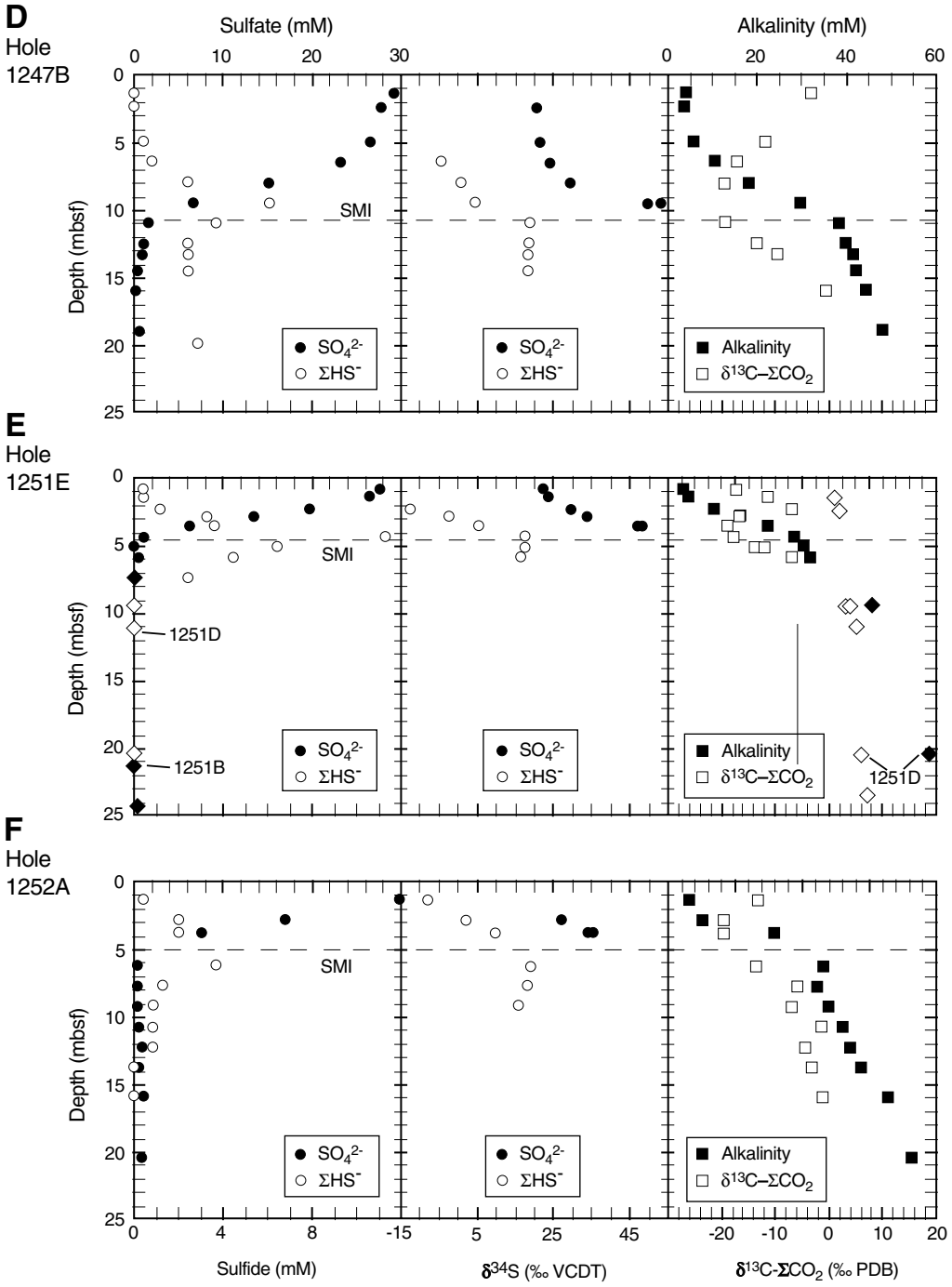

Table T1. Dissolved sulfide concentration and sulfur isotopic composition of dissolved sulfate ($\delta^{34}S–SO_4$) and sulfide ($\delta^{34}S–\Sigma HS$) along with other selected interstitial water data. (**See table notes.** Continued on next two pages.)

Core, section, interval (cm)	Depth (mbsf)	Alkalinity (mM)	$\delta^{13}C–\Sigma CO_2$ (‰ PDB)	Sulfate (mM)	Sulfide (mM)	$\delta^{34}S–SO_4$ (‰ VCDT)	$\delta^{34}S–\Sigma HS$ (‰ VCDT)
204-1244B-							
1H-1, 140–150	1.40	1.50		30.5	0.8		
1H-3, 140–150	4.40	10.55		23.5	1.6		
2H-2, 140–150	9.50	38.86		0.3			
2H-5, 140–150	14.00	44.56		0.0	2.4		
3H-2, 140–150	19.00			0.0			
3H-5, 140–150	23.50	57.37		0.0			
204-1244C-							
1H-1, 65–75	0.65	2.86	–3.1	29.7	0.0	20.0	
1H-1, 65–75	0.65		–3.2				
1H-1, 140–150	1.40	3.39		28.6	0.0	19.8	
1H-2, 65–75	2.15	4.28	–8.3	28.0	0.4	21.0	
1H-2, 140–150	2.90	6.20		26.6	0.4	21.2	
1H-3, 65–75	3.65	8.37	–15.7	24.5	0.8	21.6	
1H-3, 140–150	4.40	12.11		21.3	1.2	24.2	
1H-4, 60–70	5.10	15.54	–21.4	18.2	2.0	26.1	
2H-1, 66–75	6.15	23.72	–21.5	11.3	3.2	29.5	
2H-1, 140–150	6.90	29.40	–22.5	7.4	4.4	34.0	
2H-2, 66–75	7.65	23.82	–22.5	3.8	4.8	40.4	
2H-2, 66–75	7.65						
2H-2, 140–150	8.40	37.42	–21.3	1.5		28.2	
2H-3, 66–75	9.15		–17.2	0.9	4.4		
2H-3, 140–175	9.90	40.08		0.6	3.6	17.9	
2H-4, 66–75	10.65	40.65		0.7	3.2		
2H-4, 140–175	11.40	40.93		0.7	2.4		
2H-5, 66–75	12.15	42.82		0.5	2.4		
2H-5, 140–175	12.90	43.87		0.5	2.4		
2H-6, 66–75	13.65	46.35		0.5	0.4		
2H-6, 140–175	14.40	45.78		0.4	0.4		
2H-7, 64–74	15.14	45.56		0.5			
3H-1, 140–150	16.40	50.27		0.5			
3H-2, 140–150	17.90	51.97		1.0			
3H-3, 140–150	19.40	53.20	8.1	0.6			
3H-3, 140–150	19.40		7.4				
3H-4, 140–150	20.90						
3H-5, 140–150	22.40	55.65		0.5			
3H-6, 140–150	23.90	56.39		0.4			
3H-7, 140–150	24.84	58.43		1.1			
204-1244E-							
1H-2, 140–150	2.90	7.19		27.3	0.4		
1H-4, 140–150	5.90	25.19		11.8	1.6		
2H-1, 140–150	10.10	41.18		1.7	3.2		
2H-2, 140–150	11.60	43.05		1.4	2.8		
204-1244F-							
1H-1, 140–150	1.40	3.29		29.4	0.4		
1H-2, 140–150	2.90	6.04		25.7	1.2	21.6	
2H-1, 140–150	5.50	34.55		5.2	3.6	50.9	
2H-3, 140–150	8.50	43.71		1.9	1.6		
3H-2, 140–150	16.50	52.06		1.3			
3H-4, 140–150	19.50	56.30		1.5			
204-1245B-							
1H-2, 140–150	2.90	8.26	–15.9	24.7	0.8	21.3	
1H-5, 140–150	7.40	37.25	–24.9	1.2	3.2		
2H-2, 140–150	12.40	43.32	–11.1	0.4	4.4		
2H-2, 140–150	12.40		–10.7				
2H-4, 140–150	15.40	43.21	–2.7	0.2	2.4		
3H-2, 140–150	21.90	50.47	7.7	0.8	0.0		
3H-2, 140–150	21.90		8.3				
204-1245C-							
2H-5, 140–150	14.90	43.46		1.1	2.0		
3P–1, 20–30	17.20			1.1			
4H-5, 140–150	26.40	53.96		0.6	0.0	0.0	

Table T1 (continued).

Core, section, interval (cm)	Depth (mbsf)	Alkalinity (mM)	$\delta^{13}C–\Sigma CO_2$ (‰ PDB)	Sulfate (mM)	Sulfide (mM)	$\delta^{34}S–SO_4$ (‰ VCDT)	$\delta^{34}S–\Sigma HS$ (‰ VCDT)
204-1245D-							
1H-1, 60–70	0.60	2.95	–3.3	29.1	0.0	19.9	
1H-1, 60–70	0.60		–0.1				
1H-1, 135–150	1.35	3.66	–5.5	29.4	0.4	20.1	
1H-2, 65–75	2.15	4.89	–12.5	27.7		19.2	
1H-2, 65–75	2.15		–12.1				
1H-2, 135–150	2.85	7.07	–16.0	26.0	1.0	21.8	–3.12
1H-3, 40–50	3.40	11.44		23.1	0.8	24.2	–1.89
1H-3, 40–50				22.1		24.1	
1H-3, 85–100	3.85		–20.3		2.4		–0.83
1H-3, 85–100	3.85						
2H-1, 65–75	5.65	28.06	–24.9	7.7	3.6	40.5	8.9
2H-1, 135–150	6.35	32.42	–24.2	4.4	5.6	45.5	13.4
2H-2, 65–75	7.15	36.33	–24.6	1.4	4.0	35.1	18.2
2H-2, 135–150	7.85	37.22	–21.3	1.2	4.4	18.8	18.5
2H-3, 65–75	8.65		–18.8	1.1	4.4		18.8
2H-3, 135–150	9.35	39.23	–15.2	0.9	3.2		19.2
2H-4, 135–150	10.85	39.88	–10.4	0.6	3.2		18.2
2H-5, 135–150	12.35	40.82	–6.5	0.8	2.0		18.7
2H-5, 135–150	12.35		–6.4				
2H-6, 135–150	13.85	44.14	–3.4	0.7	1.6		17.9
3H-1, 135–150	15.85	44.60	–0.7	1.1	1.2		18.6
3H-2, 135–150	17.35	46.31	2.2	0.7	1.2		
3H-3, 135–150	18.85	47.39	4.0	1.1	1.2		
3H-4, 135–150	20.35	48.66	5.0	1.0	0.0		
3H-5, 135–150	21.85	50.32	6.3	0.8		1.0	
204-1246B-							
1H-2, 145–150	2.95		–10.1	26.1	0.8	21.3	
1H-2, 145–150	2.95		–11.7				
2H-2, 145–160	7.65	32.90	–30.2	1.6	3.2	21.7	19.3
2H-5, 145–150	12.15	35.68	–11.6	1.0	1.6		18.5
3H-2, 140–150	17.10	38.30	2.4	0.8	0.8		
3H-5, 140–150	21.60	38.18		1.0	0.4		
4H-2, 140–150	26.60	40.37		1.1	0.0		
204-1247B-							
1H-1, 140–150	1.40	3.75	–3.3	29.2	0.0		
1H-2, 90–100	2.40	3.60		27.8	0.0	20.4	
2H-1, 140–150	5.00	5.61	–11.9	26.5	0.4	21.6	
2H-2, 140–150	6.50	10.49	–17.2	23.3	0.8	24.1	–4.4
2H-3, 140–150	8.00	18.02	–19.6	15.2	2.4	29.4	1.0
2H-4, 140–150	9.50	29.34		6.8	6.1	53.1	4.4
2H-4, 140–150	9.50					49.6	
2H-5, 140–150	11.00	38.07	–19.5	1.6	3.6		18.6
2H-5, 140–150	11.00		–19.3				
2H-6, 140–150	12.50	39.60	–13.5	1.1	2.4		18.5
2H-7, 77–78	13.37	41.32	–9.6	0.8	2.4		18.4
3H-1, 140–150	14.50	41.96		0.3	2.4		18.3
3H-2, 140–150	16.00	44.11	–0.5	0.2	0.0		
3H-4, 140–150	19.00	47.98		0.5			
204-1248B-							
1H-1, 0–20	0.00	42.65	–18.5	2.2	7.7	19.1	
1H-1, 0–20	0.00		–20.0				
1H-2, 0–20	1.20	42.67	–0.9	0.2	5.6		
2H-1, 77–87	7.27	55.77	17.6	0.5	0.0		
2H-3, 91–101	9.16	59.90	18.0	0.2	0.0		
204-1248C-							
1X-1, 138–148	1.38	52.12	–21.9	0.2	6.5		
1X-1, 138–148	1.38		–25.4				
2X-CC, 0–15	10.68	54.71	15.6	1.6	0.0	18.2	
3X-1, 140–150	20.60	71.42	16.3	0.7	0.0		
204-1249C-							
1H-1, 110–118	1.10	48.31		1.7	0.0	18.8	
1H-1, 118–125	1.18	27.13		0.0	0.0		
2H-2, 0–15	3.40	41.95		0.0	0.0		
204-1249D-							
1H-2, 25–40	1.52	33.38		2.7	1.6	18.6	
3H-1, 79–94	9.79	49.91		0.6	0.0		

Table T1 (continued).

Core, section, interval (cm)	Depth (mbsf)	Alkalinity (mM)	$\delta^{13}C–\Sigma CO_2$ (‰ PDB)	Sulfate (mM)	Sulfide (mM)	$\delta^{34}S–SO_4$ (‰ VCDT)	$\delta^{34}S–\Sigma HS$ (‰ VCDT)
204-1249E-							
3H-1, 25–45	9.25				0.0		
204-1250C-							
1H-1, 0–10	0.00	39.31	14.1	0.6	0.0		
2H-CC, 1–10	5.07	64.10		0.9	0.0		
3H-2, 140–150	16.90	68.48		0.5	0.0		
3H-5, 140–150	21.40	68.02	14.6	0.0	0.0		
204-1250D-							
3H-4, 52–62	21.02	66.22		0.2	0.0		
204-1250E-							
1H-1, 140–150	1.40	39.31		1.7	10.9		
1H-2, 131–141	2.81	38.20		1.5	11.7		
2H-5, 140–150	13.90	69.07		1.4	0.0		
204-1251B-							
1H-2, 145–150	2.95	56.64	–0.5	0.7	3.6		
1H-5, 145–150	7.45	74.96	8.2	0.0	0.8		
1H-5, 145–150	7.45		8.3				
3H-2, 140–150	21.43	107.29	12.7	0.0	0.0		
3H-4, 140–150	24.41	105.16		0.4	0.0		
204-1251C-							
1H-2, 140–150	2.90	27.31			2.8		
1H-5, 140–150	7.40	59.61			0.0		
2X–1, 140–150	9.50	71.98			0.0		
2X–3, 140–150	12.07	88.49			0.0		
204-1251D-							
1X–1, 140–150	1.40	30.30	–17.4	11.1	4.0	40.2	5.6
1X–2, 90–100	2.40	48.85	–17.4	0.8	6.1		18.4
2X–1, 140–150	9.50	75.43	7.2	1.1	0.0		
2X–1, 140–150	9.50		7.6				
2X–3, 50–60	11.10				0.0		
3X–2, 140–150	20.50	97.21	11.6	0.9	0.0		
204-1251E-							
1H-1, 85–95	0.85	5.80	–17.4	27.5	0.4	22.4	
1H-1, 85–95	0.85		–17.2				
1H-1, 140–150	1.40	7.50	–11.6	26.6	0.4	23.4	
1H-1, 140–150	1.40		–11.4				
1H-2, 80–90	2.30	16.81	–7.0	19.6	1.2	29.7	–12.7
1H-2, 140–150	2.90	26.88	–17.0	13.5	3.2	33.6	–2.4
1H-3, 60–70	3.60	37.47	–18.8	6.2	3.6	47.2	5.3
1H-3, 60–70	3.60					48.0	
1H-3, 140–150	4.40	47.10	–17.8	1.0	11.3		17.7
1H-4, 60–70	5.10	50.63	–12.2	0.0			17.4
1H-4, 60–70	5.10		–13.6		6.5		
1H-4, 140–150	5.90	52.81	–6.9	0.5	4.4		16.5
1H-5, 140–150	7.40				2.4		
204-1252A-							
1H-1, 135–150	1.35	7.60	–9.9	29.8	0.4		–8.2
1H-2, 135–150	2.85	12.91	–17.7	16.9	2.0	27.2	2.0
1H-3, 85–100	3.85	39.98	–17.4	7.5	2.0	34.1	9.6
1H-3, 85–100	3.85					35.3	
2H-1, 135–150	6.25	57.84	–10.3	0.4	3.6		18.9
2H-2, 135–150	7.75	55.57	–1.1	0.4	1.2		18.1
2H-3, 135–150	9.25	59.62	–2.3	0.3	0.8		15.6
2H-4, 135–150	10.75	65.07	4.1	0.5	0.8		
2H-4, 135–150	10.75		4.4				
2H-5, 135–150	12.25	68.01	0.8	0.9	0.8		
2H-6, 135–150	13.75	71.93	2.0	0.5	0.0		
3H-2, 135–150	16.00	82.09	4.6	1.1	0.0		
3H-5, 135–150	20.50	90.61		0.9	0.0		

Notes: Sulfate concentration and alkalinity data are from Tréhu, Bohrmann, Rack, Torres, et al. (2003). Carbon isotopic composition of dissolved carbon dioxide ($\delta^{13}C–CO_2$) is from Torres and Rugh (this volume). mM = millimoles per liter. VPDB = Vienna Peedee Belemnite. VCDT = Vienna Canyon Diablo Troilite.